Journal of Materials Chemistry A

PAPER

Cite this: J. Mater. Chem. A, 2015, 3, 5375

Fully indium-free flexible Ag nanowires/ZnO:F composite transparent conductive electrodes with high haze†

Jun Han,[a] Shuai Yuan,[a] Lina Liu,[a] Xiaofeng Qiu,[a] Haibo Gong,[a] Xiaopeng Yang,[a] Cuncheng Li,[a] Yufeng Hao[b] and Bingqiang Cao*[a]

Received 26th October 2014
Accepted 15th January 2015

DOI: 10.1039/c4ta05728g

www.rsc.org/MaterialsA

Solution-processed metal nanowires (NWs) and Earth-abundant doped ZnO have been proposed to replace the most widely used indium tin oxide (ITO) transparent and conductive electrode. Generally, there is a dilemma, the trade-off between optical transparency and conductivity for these materials taken alone makes them difficult to compete with commercial ITO. In this work, a modified polyol synthesis method was adopted to grow single-crystal silver nanowire with controlled length by adding $AgNO_3$ solution in advance and using high molecular weight polyvinylpyrrolidone (PVP). Ag nanowires ink was then spin coated onto flexible PET substrate to form Ag NW mesh, which shows impressive transparent and conductive (TC) property with sheet resistance of 23 Ω sq^{-1} and transmittance of 90.4% at a wavelength of 550 nm. A post fluorine-doped ZnO (FZO) layer was then deposited by pulsed laser deposition method to improve the TC, stability and mechanical property. High-quality Ag NW/FZO composite electrode was finally acquired at room temperature after optimizing the Ag NW length, concentration in suspension, and FZO layer thickness, with transmittance of 83% at wavelength of 550 nm, sheet resistance of 17 Ω sq^{-1}, and high haze of 36.5%. Perovskite solar cells incorporating such Ag NW/FZO composite electrode exhibited a better cell performance compared to the similar FTO-based perovskite solar cells.

1. Introduction

Transparent conducting electrodes (TCEs), which possess high conductivity and high transparency are widely used as the critical components of various optoelectronic devices, such as solar cells (SCs),[1] light-emitting diodes (LEDs),[2] and touch screen panels.[3] The most popular TCE materials to date are transparent conductive oxides. In particular, tin doped indium oxide (ITO) is the most widely used TCE material in above applications, for its excellent transparent conductive performance (10–20 Ω sq^{-1} at 85–90% transmittance).[4] However, ITO suffers from major limitations, such as scarcity and high cost of indium, high temperature processing for deposition and inherent brittleness, which restrict ITO to the application for next-generation flexible and low-temperature processible optoelectronic devices.[5] Therefore, there is an urgent need to develop new indium-free and easy-to-handle TCE materials for future flexible optoelectronic devices. Various emerging nanomaterials, such as carbon nanotubes (CNT),[6] graphene,[7] metal grids or metal nanowires (NW) mesh[8,9] have been studied as promising candidates. Though carbon-based nanomaterials are abundant, the graphene and carbon nanotube films have a typical sheet resistance of 100–200 Ω sq^{-1} at 80–90% transmittance, which is too high compared with ITO.[10] Meanwhile, graphene and carbon nanotubes are considered too difficult to grow on large scale.[11] Alternatively, TCEs based on metal grids or random nanowires network[12] have attracted considerable attention. Lee *et al.*[13] first demonstrated silver nanowires (Ag NW) TCEs on glass substrate using the solution dispersed Ag NWs, prepared by the polyol reduction method that was developed by Sun *et al.*[14] Particularly, Ag NW TCEs has many advantages, such as high transparency (80–90%), high conductivity (15–25 Ω sq^{-1}), mechanical flexibility, and solution processability, which are reported to compete with the TC properties of ITO.[15] Furthermore, Ag NW TCEs has potentials for large-scale commercial production, owing to solution-based process, such as roll-to-roll printing, spraying and spin-coating.[16] However, there are also some severe drawbacks of pristine Ag NW TCEs including weak mechanical adhesion to the substrate and oxidation of silver, which limits their application to optoelectronic devices.[17] In addition, Ag NW TCEs

[a]Key Lab of Inorganic Functional Material in Universities of Shandong, School of Material Science and Engineering, School of Chemistry and Chemical Engineering, University of Jinan, Jinan 250022, China. E-mail: mse_caobq@ujn.edu.cn; Fax: +86-531-8973-6292; Tel: +86-531-8973-6292

[b]Department of Mechanical Engineering, Columbia University, New York, NY 10027, USA

† Electronic supplementary information (ESI) available. See DOI: 10.1039/c4ta05728g

must be able to contact to all over the active area of the device for efficient charge extraction/injection in order to apply to photoelectric devices.[16] Therefore, an effective transparent and conductive medium layer is necessary on top of Ag NW mesh to develop composite electrode for overcoming the above intrinsic problems of Ag NW electrodes.

Recently, a considerable number of attempts have been made on Ag NW composite electrode to produce high performance ITO-free devices. Huang's group developed a double layer structured high-performance composite electrode with percolating network of Ag NW mesh and graphene.[18] However, it is complex to grow and transfer graphene uniformly onto Ag NW mesh. In addition, there are several attempts combining the Ag NW mesh with organic conductive PEDOT:PSS film.[19,20] But, researchers have demonstrated that PEDOT:PSS has detrimental effects on device lifetime.[20] Alternatively, metal oxide nanoparticles (NPs) like ITO–NP, ZnO–NP are also adapted to improve the Ag NW mesh TC performance.[21–24] Unfortunately, Ag/NPs composite TCEs sometimes need a post high-temperature (100–200 °C) annealing process, and is not suitable for the low-temperature fabrication of flexible devices.[21–24] Recently, Hyun *et al.* demonstrated that an effective indium-doped zinc oxide buffer layer on Ag NW mesh can effectively solve the intrinsic problems of Ag NW mesh, obtaining flexible and highly stable TC composite electrodes.[11] However, these composite electrodes are still somewhat related to indium.

Besides transmittance and conductivity, optical haze is an equally important parameter of TCEs, especially for improving the efficiency of solar cells. Larger haze of TCE could increase scattering and hence increase optical path length and improve light absorption, which are both important for photovoltaic devices. Fang *et al.* developed a novel transparent paper made of wood fibers with ultrahigh haze that can be used as substrate for high-efficiency solar cells.[25] Preston *et al.* investigated the effect of the NW diameter on the optical haze values of Ag NW films[26] and also reported a novel Ag nanowire paper hybrid electrode showing greater light absorption than ITO due to the higher optical haze.[27] Chen *et al.* reported the efficiency of hybrid Si/PEDOT:PSS heterojunction solar cells was improved when the haze of PEDOT:PSS film was enhanced by further covering an Ag NW mesh.[12]

Hence, in this work, a fully indium-free newly-designed flexible transparent conductive composite electrode based on effective fluorine doped ZnO (FZO) layer on Ag NW mesh both grown at room temperature is demonstrated. We studied the influence of Ag nanowire's length, Ag NW ink concentration, and FZO layer thickness on the transparent conductive properties of the composite electrodes. By comparing different types of composite electrodes grown with various conditions, the optimal Ag NW/FZO composite electrode shows transmittance of 83% at a wavelength of 550 nm with sheet resistance of 17 Ω sq^{-1} and haze of 36.5%, which are desired for next-generation flexible optoelectronic devices processed at low temperature. We also studied systematically temperature-dependent sheet resistance, mechanical adhesion and bending stability of such Ag NW/FZO composite electrodes. Furthermore, as a principle demonstration, such Ag NM/FZO electrodes were adopted as TCEs for perovskite solar cells that showed better performance than the FTO-based cells.

2. Experimental section

2.1 Synthesis of Ag NW

Regular-short silver nanowires are synthesized by reducing $AgNO_3$ with ethylene glycol (EG) in the presence of polyvinylpyrrolidone (PVP, K-30, $M_w \approx 40\,000$).[28] A 10 mL EG solution of 0.1 mM $FeCl_3$ is vigorously stirred after the addition of 0.15 M PVP. The mixed solution is injected drop by drop using a syringe into 10 mL of a magnetically stirred EG solution of $AgNO_3$ (0.1 M). Afterwards, the solution is put into a 50 mL Teflon-lined autoclave tube. This tube is sealed and maintained at 160 °C for 2.5 h, followed by natural cooling to room temperature (25 °C). The cool solution is then centrifuged three times at 6000 rpm for 15 min to remove solvent (EG), PVP, and other impurities in the supernatant. Then, they are dispersed in ethanol for further application.

The Ag NWs with high aspect ratio are synthesized by a simply modified method mentioned above. A 10 mL EG solution of 0.1 mM $FeCl_3$ is vigorously stirred after the addition of 0.15 M PVP with high molecular weight ($M_w \approx 1300\,000$), and is named as solution (1). Next, 10 mL EG solution of $AgNO_3$ (0.1 M) is stirred to uniformity in a flask as Solution (2). Then, 18 μL Solution (2) is taken with a pipette and dipped into the flask of Solution (1) stirred at 95 °C for 5 min for initial nucleation of the silver seeds. The mixed solution becomes yellowish first and then becomes milky white. Next, the remaining Solution (2) is injected drop by drop using a syringe within 7 min. Then, the flask is stirred at 110 °C for 5 min. At last, the obtained solution is put into a 50 mL Teflon-lined autoclave tube, which is sealed and maintained at 160 °C for 2.5 h. The cooled solution is then centrifuged three times at 4000 rpm for 15 min to remove solvent and impurities for further application.

2.2 Preparation of Ag NW mesh and Ag NW/FZO composite electrodes

Ag NW mesh is prepared by spin-coating. Ag NW ink is dropped on the surface of flexible PET substrates. The transmittance and sheet resistance of the Ag NW mesh was expected to be controlled by changing the rotation speed, the concentration of Ag NW ink, and also the Ag NW itself. According to our experience, we optimized the rotation speed to 3500 rpm for 40 seconds. Next, plasma cleaning (PDC-32G-2, Harrick) for one minute is employed to eliminate the PVP adhering to the surface of the Ag NW for improving the conductivity.

For comparison, fully indium-free FZO layers with various thicknesses were then deposited on the Ag NW mesh by pulsed laser deposition (PLD) at room temperature. An energy density of 1 J cm^{-2} from a KrF 248 nm excimer laser, working pressure of 0.5 Pa, and target–substrate distance of 6 cm are set for PLD growth of FZO film. The FZO layer could be expected to effectively prevent undesirable electrical and chemical changes of the Ag NW composite electrodes, improve the adhesion and bending stability, and realize contacting to all over the active

area of the device to allow for efficient charge extraction/injection. The details will be discussed in the paper.

2.3 Structure and property characterizations

Morphology and crystal structure studies of the Ag NW based electrodes were performed with a field emission scanning electron microscope (FESEM, Quanta 250, FEI), transmission electron microscope (HRTEM, JEM-2100F, JEOL), and X-ray diffraction (XRD, D8-Advance, Bruker), respectively. The transmittance spectra were measured using a UV-vis-NIR spectrophotometer (UV-3600, Shimadzu) equipped with an integrating sphere. The sheet resistances were measured by a four-point probe method with a source/meter (Keithley 2162A) and probe station (ECOPIA, ESP300). Temperature-dependent sheet resistances were measured on a home-made resistivity measurement probe kit with a 45 K closed cycle refrigerator systems from CTI-Cryogenics.

2.4 Preparation and characterization of perovskite solar cells

To investigate the feasibility of the Ag NW/FZO composite electrodes as TCE for solar cells, we fabricated perovskite solar cell on FTO substrates and Ag NW/FZO substrates. Except for the transparent electrode, all layers in the devices were fabricated under identical processing conditions. A TiO_2 hole-blocking layer was deposited onto the substrates *via* PLD at 70 °C for a quarter of an hour.[29] Then, the substrates were transferred to a vacuum evaporator chamber to grow PbI_2 (130 nm) films. The PbI_2 was then reacted with a solution of CH_3NH_3I in 2-propanol in a home-made closed vessel for 3 minutes in a glovebox. Then, the obtained $CH_3NH_3PbI_3$ perovskite was annealed at 120 °C for 20 min in N_2 atmosphere. The hole transporting materials (HTM) were prepared by dissolving 72.3 mg spiro-MeOTAD, 28.8 μL 4-*tert*-butylpyridine, 17.5 μL of a stock solution of 520 mg mL^{-1} lithium bis(trifluoromethylsulphonyl)imide in acetonitrile in 1 mL chlorobenzene and then deposited by spin coating at 3000 rpm for 30 s. Finally, silver pads with an area of 10 mm^2 were deposited on top of the device to form the back contacts using a thermal evaporator under a pressure of 10^{-6} Torr. The current density–voltage (*J–V*) curves were measured using a Keithley 2612A source measurement unit, and photovoltaic performance was measured under an illumination intensity of 100 mW cm^{-2} using a San-Ei solar simulator at AM 1.5G conditions.

3. Results and discussion

3.1 Ag NW TC performance controlled by length

The final color of Ag NW solution synthesized in an EG solution by using PVP with molecular weight of 40 000 and 1 300 000 appears as ocher and deep ocher, which is definitely diverse from the color of Ag NPs. SEM images show that both the products were dominated by NWs with uniform diameter (Fig. 1(a and b)). The mean diameter of these as-synthesized Ag

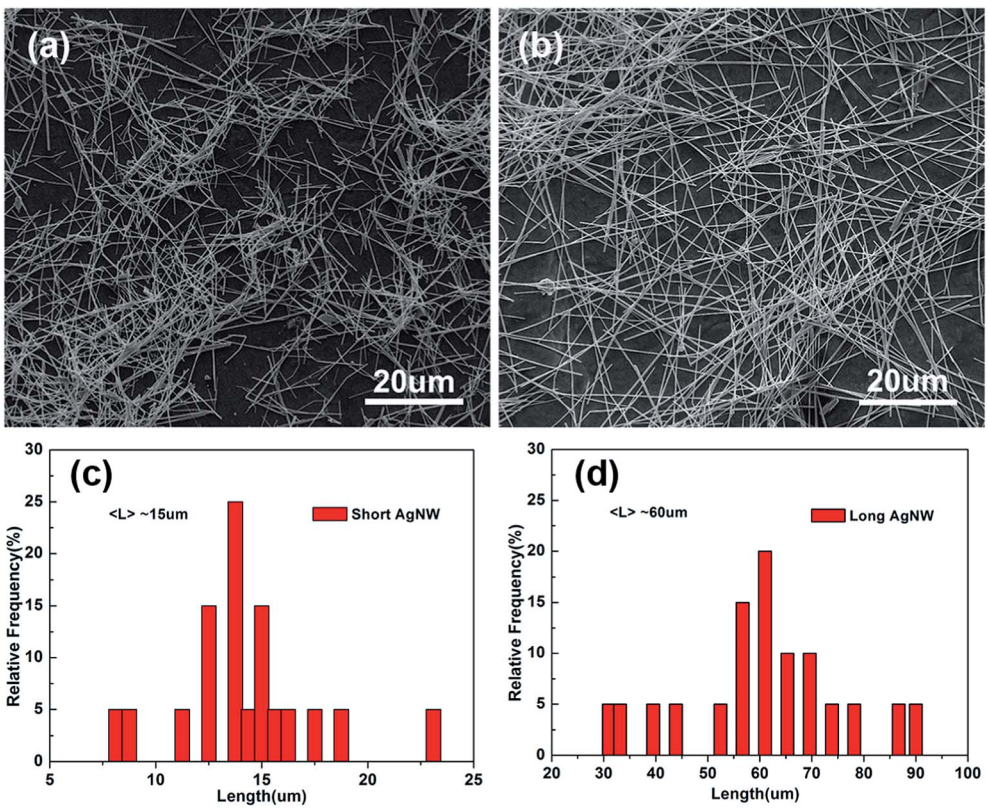

Fig. 1 (a and b) SEM images of the corresponding Ag NWs with different lengths. (c and d) Histogram of statistics relate to the length of the Ag NW.

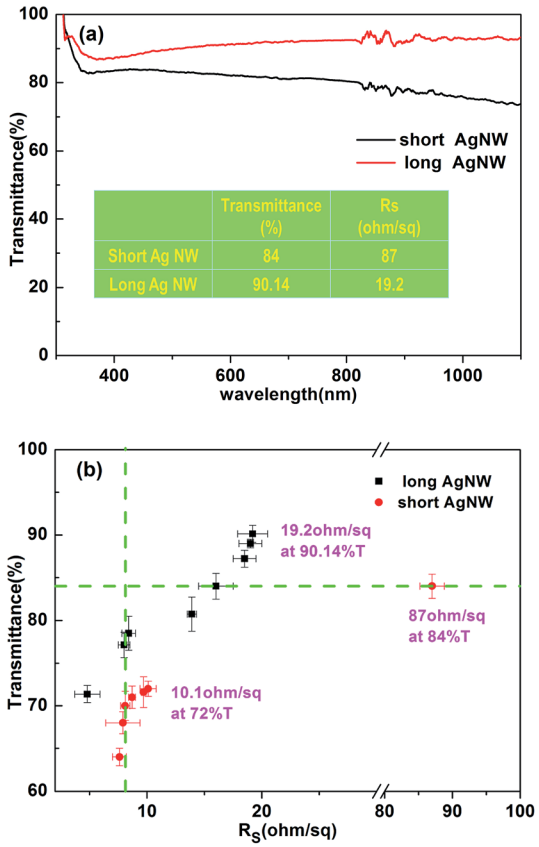

Fig. 2 (a) Transmittance curves of the optimal Ag NW meshes on PET substrates and (b) transmittance *vs.* sheet resistance plot of Ag NW meshes based on the long and short Ag NWs.

NWs is about 100–150 nm. Their primary differentia is the length. The average length of Ag NWs synthesized using PVP with a molecular weight $M_w = 40\,000$ is about 15 μm according to length statistics on over fifty nanowires (Fig. 1(c)). When surfactant PVP with $M_w = 1\,300\,000$ was used instead, the final product is dominated by Ag NWs with average length of ~60 μm (Fig. 1(d)), suggesting that PVP with a higher molecular weight favors for the growth of long Ag NWs. Ag NWs synthesized by our method grew along ⟨220⟩ direction, bound by {002} planes as the lateral surfaces (see ESI†), which is in accordance with both experimental observations and simulations of former reported Ag NWs.[14,30] Importantly, this provides us a facile and effective route to selective fabrication of Ag NWs with various lengths by selecting surfactant PVP with different molecular weight.

For device applications like large-size displays and solar cells, low sheet resistance and high transmittance of TCEs are both important. Fig. 2(b) shows that the transmittance improves while the sheet resistance increases, for these two kinds of Ag NW TCEs. Moreover, for a given sheet resistance, the transmittance increased with NW length.[31,32] For example, at an $R_S \sim 8.1\ \Omega\ sq^{-1}$, the transmittance of the films composed of 60 μm NW (~80%) is much higher than films composed of 15 μm NW (~68%). The possible reasons can be explained with two-dimensional widthless stick model that can be simulated with Monte Carlo method. For sticks with a given length (L), the critical number density (N_c) of sticks required for percolation is given by eqn (1) (ref. 33)

$$N_c L^2 = 5.71. \quad (1)$$

This equation indicates that longer nanowires will make for qualitatively better transparent conducting films. As the length of the NW increases, the number density of nanowires necessary to achieve a given sheet resistance decreases, which results in a higher transmittance.[34] Therefore, long Ag NW is a better choice compared with short Ag NW, for transparent conductive electrode applications.

3.2 Ag NW TC performance controlled by ink concentration

The relationship between sheet resistance and transmittance of Ag NW meshes with the Ag NW ink concentration was further investigated. Fig. 3 shows Ag NW films with different densities on PET substrates coated with various concentration of Ag NW ink. Fig. 3(a) is a SEM image for a 10.8 mg mL^{-1} Ag NW mesh. There are fewer holes in the films, which could lead to more uniform electrical field distribution when used in optoelectronic devices. By tuning the density, we can achieve sheet resistance as low as 4.8 Ω sq^{-1} (Sample A), which precedes the performance of commercial ITO film on plastic substrate (~20 Ω sq^{-1}). As the concentration of Ag NW ink decreases continually, the nanowire become sparse with some holes in the film, as shown in Fig. 3(c–f), which contributes to improve the transmittance achieving as high as 90–92%. However, the sheet resistance clearly increases with decreased concentration of Ag nanowire ink as summarized in Table 1. Though the holes or openings in the Ag NW film could be a problem for device applications, designing composite electrode structure may solve the problem for better electrical field distribution,[35] as will be discussed below.

As expected, the transmittance increases when a smaller concentration of Ag nanowire ink is coated. But, it also results in an increased sheet resistance because a smaller amount of nanowires is used to form the mesh. As shown in Fig. 3(h), the transmittance of the Ag nanowires at a wavelength of 550 nm is plotted against the respective sheet resistance. The transmittance for sheet resistance of 19.4 Ω sq^{-1} is measured to be 90.14% for our Ag nanowires (Sample F), whereas that of ITO is 89.8%.[36] The transmittance data for different nanowire densities is shown in Fig. 3(g). It is clear that the transmittance increases due to the decrease in the concentration of Ag NW ink. Furthermore, the high transmittance of our Ag NW meshes can keep nearly constant from ultraviolet to near infrared wavelength, which can improve the utilization range of light when applied as the window layer of the solar cell. Therefore, Ag NW meshes are more suitable as TCEs than ZnO:Al (AZO) to enhance the spectral response at the near-infrared to infrared regime, where the free carrier absorption coefficient of AZO film is very high.[37]

The figure of merit (FoM) is a typical parameter commonly used to evaluate transparent conductive electrodes, which

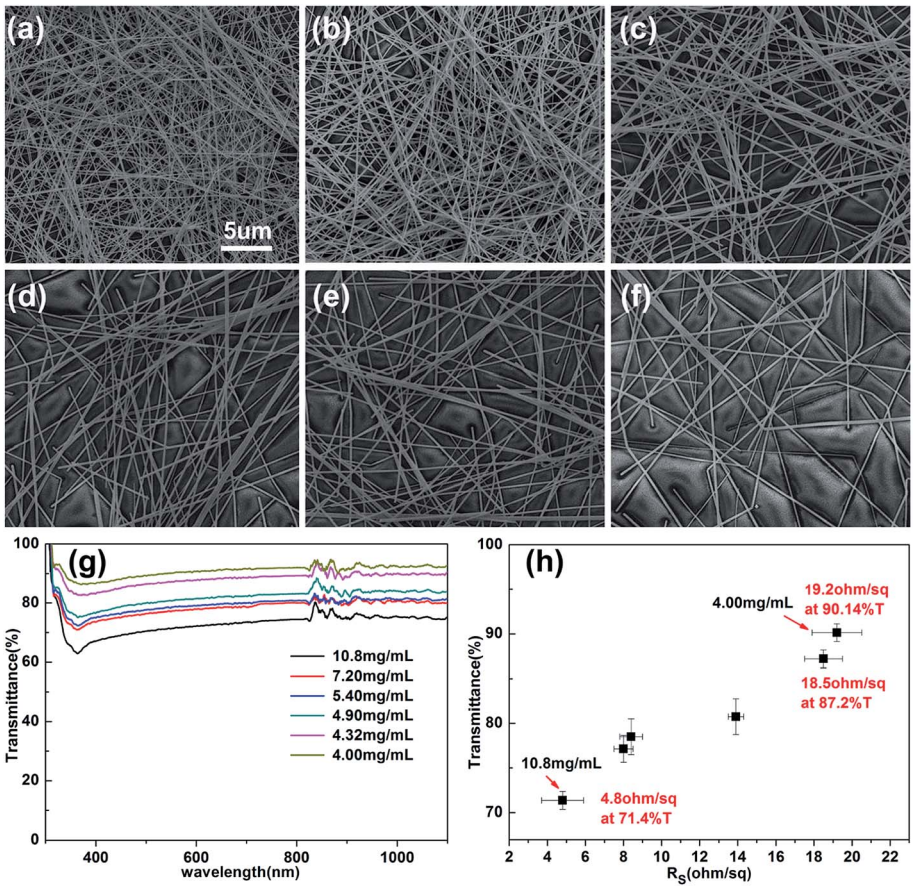

Fig. 3 SEM images of the long Ag NW meshes coated with Ag NW ink of various concentrations, (a) 10.8 mg mL^{-1} (b) 7.2 mg mL^{-1} (c) 5.4 mg mL^{-1} (d) 4.9 mg mL^{-1} (e) 4.32 mg mL^{-1} (f) 4.0 mg mL^{-1}. Accordingly, the samples are named as Sample A–F, respectively. (g) Shows the corresponding transmittance spectra and (h) compares the transmittance *vs.* sheet resistance data.

Table 1 Figure of merit (FoM) of the Ag NW meshes with various concentration of Ag NW ink

Ag NW meshes	R_s (Ω sq^{-1})	Figure of merit ($\times 10^{-3}$)
Sample A (10.8 mg mL^{-1})	4.8	7.14
Sample B (7.20 mg mL^{-1})	8	9.33
Sample C (5.40 mg mL^{-1})	8.4	10.6
Sample D (4.90 mg mL^{-1})	13.9	8.5
Sample E (4.32 mg mL^{-1})	18.5	13.7
Sample F (4.00 mg mL^{-1})	19.2	18.4

applies to optimize electrode designs.[11] The FoM is calculated with the sheet resistance (R_s) and the optical transmittance (T) at a wavelength of 550 nm as defined by Haacke[38]

$$\text{Figure of merit} = T^{10}/R_s. \quad (2)$$

FoM of neat Ag NW meshes can be controlled by changing the concentration of Ag nanowire ink. As shown in Table 1, with the decrease in concentration, the overall trend of FoM of neat Ag NW meshes is increasing. The FoM of Ag NW meshes for Sample F is measured to be 18.4×10^{-3}, which is comparable or even higher than the reported values $\sim 8.8 \times 10^{-3}$ of ITO.[34] This indicates high-performance pristine Ag NW meshes can be prepared by controlling the concentration of Ag NW ink.

3.3 Ag NW TC performance enhanced by post FZO film deposition

The effects of post FZO layer coating and their thickness on the transparent conductive properties of the composite electrodes was further studied. In order to compare our newly designed composite electrode, we have listed the corresponding transmittance, sheet resistance, optical haze and FoM values of various types of Ag NW/FZO films in Table 2. It is obvious that post FZO layer coating can effectively decrease the sheet resistance of Ag NW films, but the transmittance also decreases due to the absorption of FZO. Fig. 4 compares the typical transmittance and optical haze curve of the composite Ag NW/FZO (100 nm) electrode and a corresponding neat Ag NW mesh. The Ag NW/FZO (100 nm) composite electrode shows above 83% transmittance in the visible wavelength region and can keep to near infrared region. The optical haze of the Ag NW/FZO (100 nm) composite electrode is about 36.5% at a wavelength of 550 nm, which is higher than the reported data (~25%) of transparent conductive ZnO:Al film with highly textured surface.[39]

Table 2 Transparent conductive properties, optical haze values of the pristine Ag NW meshes and Ag NW/FZO composite electrodes with various thicknesses of FZO layers

	Ag NW	Ag NW/FZO (50 nm)	Ag NW/FZO (100 nm)	Ag NW/FZO (150 nm)	Ag NW/FZO (300 nm)
R_{sh} (Ω sq^{-1})	23	22	17	15.2	13.3
$T_{at\ 550\ nm}$ (%)	90.4	85	83	79	67
Haze$_{at\ 550\ nm}$ (%)	38	37.7	36.5	36.4	37.5
Figure of merit ($\times 10^{-3}$)	15.2	8.95	9.13	6.23	1.37

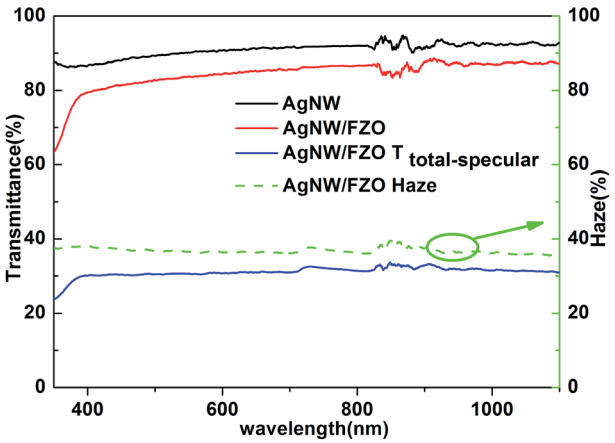

Fig. 4 Transmittance and optical haze comparison of a typical Ag NW mesh and the corresponding Ag NW/FZO (100 nm) composite electrode coated on PET substrates.

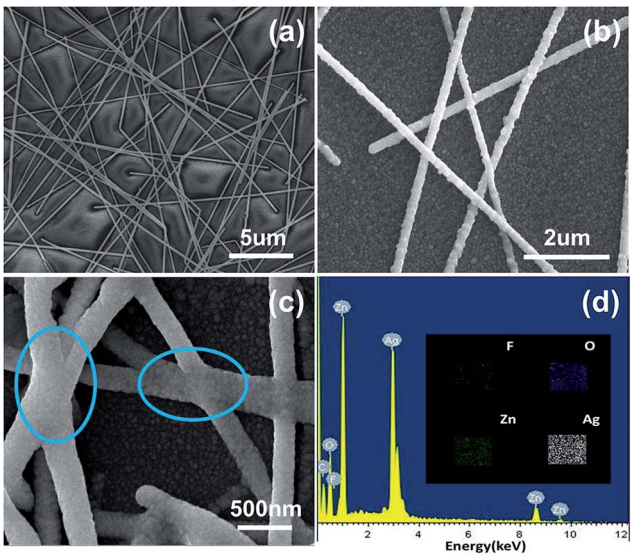

Fig. 5 SEM images of (a) the random Ag NW mesh, (b) Ag NW/FZO (50 nm) and (c) Ag NW/FZO (100 nm) welded composite electrodes. (d) EDX spectrum showing the elemental composition of the Ag NW/FZO (100 nm).

To understand the roles of FZO layer, the Ag NW/FZO composite films were characterized with SEM. Fig. 5 shows SEM images both before and after deposition of the FZO layer. For pristine Ag NW mesh, the connection between crossed Ag NW is mainly by physical contact, *via* van der Waals forces between Ag NWs, and capillary force from solvent evaporation.[17] Thus, the Ag NW mesh appear loose connections without forming junctions, as shown in the SEM image of Fig. 5(a). In Fig. 5(b), the Ag NW mesh is coated with a FZO (50 nm) layer. A FZO layer formed on the entire plane is clearly observed. Particularly, Ag NWs weld together at their crossing points with FZO coating layer. However, a FZO layer of 50 nm is thin and weak that cannot provide strong adhesion and weld. Thus, it fails to effectively decrease sheet resistance, as shown in Table 2. Therefore, we increase the thickness of the FZO layer to 100 nm as shown in Fig. 5(c). The FZO layer can achieve a very effective fusion between Ag NW on their crossing points as indicated with cycles in Fig. 5(c) and the R_{sh} reduced from 23 Ω sq^{-1} for the Ag NW mesh to 17 Ω sq^{-1}. Continuing to increase the thickness of the FZO layer, the NW crossing points are basically unchanged (SEM images not shown here). Although such Ag NW/FZO electrodes with thicker FZO layers have a characteristic of high conductivity, the low transmittance as summarized in Table 2 is not preferred for further application as TCEs. Thus, the optimized FZO layer in our case is about 100 nm.

The FoM value of Ag NW/FZO composite electrode becomes larger when the thickness of FZO layer increase from 50 nm to 100 nm. However, it begins to decrease with the thickness of FZO layer further increasing from 100 nm to 300 nm. The reason is that although FZO layer decreases sheet resistance of Ag NW films, but the large decrease of transmittance from 90.4% to 67% (Table 2) results in a smaller FoM value. Therefore, by comparing different composite electrodes with various thickness of FZO layer, the Ag NW/FZO (100 nm) film is the optimal composite electrode with a larger FoM.

Temperature dependence of the sheet resistance of Ag NW/FZO composite electrode was further measured to understand the roles of FZO layer and Ag NW mesh. The sheet resistance of the Ag NW/FZO composite electrodes decreased with decreasing temperature from 300 K to 60 K as shown in Fig. 6. The temperature coefficient of the sheet resistance is positive during sample cooling and heating, as opposed to the tendency of doped-ZnO film, as shown in the inset. Regardless of heating or cooling from 300 to 60 K, the Ag NW/FZO composite electrodes exhibited similar temperature coefficients of the sheet resistance, indicating that the Ag NW/FZO composite electrode possessed a typically metallic conduction mechanism in

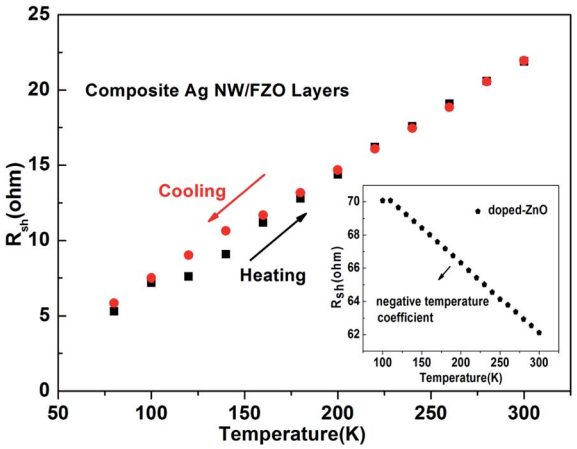

Fig. 6 Temperature-dependent sheet resistance of Ag NW/FZO composite electrode and doped-ZnO film (inset).

electrical transport properties due to existence of metallic Ag NW mesh. Therefore, the electrical properties of the Ag NW/FZO composite electrode were mainly dominated by Ag NW network. Thus, the main effect of FZO layer coating on the electrical conductivity is the formation of effective fusion between Ag NWs on their crossing points and larger contact areas to improve the electrical properties.

Although electrode transparency and conductivity are important characteristics for high performance TCEs, the haze factor of TCE, for solar cell application, is another critical contributor to the cell efficiency.[25] The haze factor is defined as the forward scattering transmittance ($T_{total} - T_{specular}$) divided by the total transmittance (T_{total}) and can be calculated as[5,25]

$$\text{Haze}\ (\%) = (T_{total} - T_{specular})/T_{total} \quad (3)$$

The T_{total} and $T_{specular}$ are total transmittance and specular transmittance, respectively. The optical haze value of our Ag NW based composite electrodes is as high as 36.4–38% (Table 2). These haze value are higher than the reported values of Ag NW mesh from Kim *et al.* (~15%)[5] and Hu *et al.* (~31%).[10] Furthermore, our newly designed composite electrodes have nearly identical large optical haze factor, which are suitable for TCE in solar cells.

3.4 Perovskite solar cells with Ag NW/FZO composite TCEs

To directly evaluate the potential use of Ag NW/FZO composite film as transparent electrode for solar cells, we fabricated perovskite solar cells on both Ag NW/FZO substrates and FTO substrates for comparison. The reference solar cells are fabricated on the commercial FTO glass substrates with 18–20 Ω sq^{-1} at 82–83% transmittance and 14–16% of haze value, which is widely used as electrode of perovskite solar cells.[40–43] The

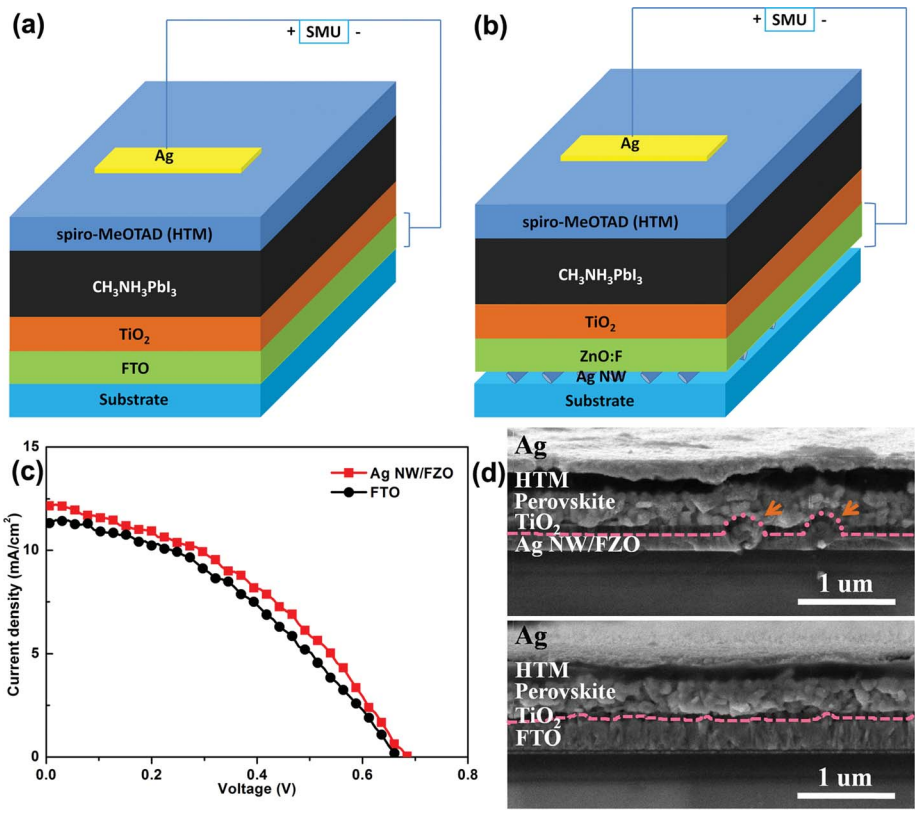

Fig. 7 (a and b) Schematic structures of perovskite solar cells using different transparent conductors such as FTO and Ag NW/FZO electrodes. All of the other layers such as the absorber are identical. (c) Current density–voltage characteristics for the perovskite solar cells based on the various electrodes. (d) Cross-sectional SEM micrographs of solar cells.

Table 3 Performance comparison of perovskite solar cells fabricated on FTO and Ag NW/FZO electrodes

	J_{sc} (mA cm^{-2})	V_{oc} (V)	FF (%)	PCE (%)
FTO	11.4	0.667	38.8	2.95
Ag NW/FZO	12.2	0.685	39.5	3.29

schematic structures of TiO_2/$CH_3NH_3PbI_3$/spiro-MeOTAD/Ag perovskite solar cells using FTO and Ag NW/FZO electrode are shown in Fig. 7(a) and (b). Except for the transparent electrode, the device structure was fabricated under identical processing conditions, as shown in Fig. 7(d) with the cross-sectional SEM micrographs. The current density–voltage (J–V) curves of the perovskite solar cells based on different transparent electrodes were measured under 100 mW cm^{-2} illumination (AM 1.5G condition), as shown in Fig. 7(c). Their photovoltaic performance data are summarized in Table 3. As shown in Fig. 7(c) and Table 3, the perovskite solar cells fabricated on the reference FTO transparent electrode showed typical performance: a FF of 38.8%, a J_{sc} of 11.4 mA cm^{-2}, a V_{oc} of 0.667 V, and a PCE of 2.95%. Although these values are relatively lower than the values reported for perovskite solar cells,[44,45] the TiO_2/$CH_3NH_3PbI_3$/spiro-MeOTAD/Ag could serve as a platform to compare the influence of the transparent electrodes. The perovskite solar cells with the Ag NW/FZO electrode showed improved cell-performance: a FF of 39.5%, a J_{sc} of 12.2 mA cm^{-2}, a V_{oc} of 0.685 V, and a PCE of 3.29%. These results are quite comparable to the reference devices on FTO substrates. But, efficient perovskite solar cells based on Ag NW/FZO electrode are achieved. Higher J_{sc} and PCE values were observed compared to the reference cell with FTO electrode. This mainly could be ascribed to the relatively low sheet resistance and high haze value of Ag NW/FZO electrode. The low sheet resistance makes it possible to effectively transport the charge carriers generated in the solar cell to the front contact, reducing the current loss at the electrode.[35] The high haze value presenting a large scattering of light by Ag NWs can enhance the light absorption in the solar cell, resulting in higher PCE and J_{sc}, as discussed by Kim *et al.*[1] Thus, the higher haze value together with smaller sheet resistance of Ag NW/FZO may be responsible for the improved cell performance. Therefore, it is believed that Ag NW/FZO electrodes may be more promising transparent conductive electrodes for solar cells.

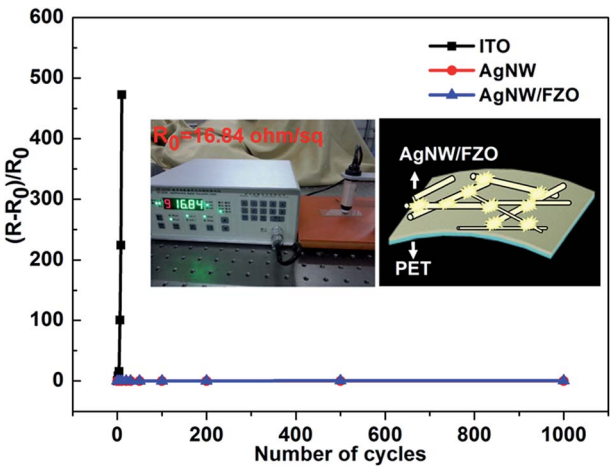

Fig. 8 $(R - R_0)/R_0$ *vs.* the number of cycle for the various electrodes on PET. The inset shows the R_0 and schematic diagram of the bending Ag NW/FZO composite electrode.

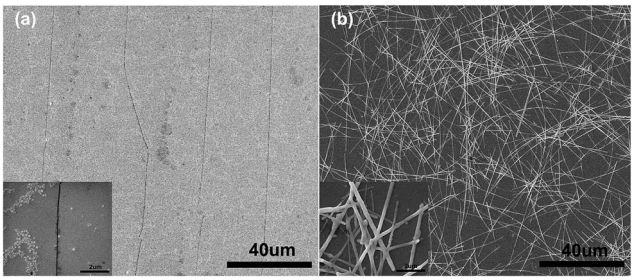

Fig. 9 SEM images of the typical ITO and Ag NW/FZO composite electrode after bending test: (a) ITO, after 10 bending cycles; (b) Ag NW/FZO composite electrode, after 10 3 bending cycles. The insets show partial enlarged detail of the ITO and Ag NW/FZO composite electrode after bending test.

3.5 Flexibility and stability test of Ag NW/FZO composite TCEs

The flexibility and stability of TCEs are also two important properties for long-life flexible electronics. Fig. 8 shows the flexibility test results of Ag NW/FZO composite electrode, pristine Ag NW mesh, and commercial ITO film on PET substrates (35 Ω sq^{-1} at 85% transmittance, Kaivo Optoelectronic Technology). The bending test is carried out for 1000 times at a frequency of 1 Hz and with a bending length and radius of 15 mm and 5 mm, respectively. As expected, the ITO film fails to maintain the flexibility and the $(R - R_0)/R_0$ of the ITO film changes by 473% after ten bending cycles. In contrast, the composite Ag NW electrode exhibits a stable electrical performance, even after more than 1000 bending tests. Its ability to endure hundreds of cycles of mechanical bending test is due to the flexibility of the Ag NW mesh built with long Ag NWs and the strong adhesion by forming effective fusions between Ag NWs at their numerous crossing points. Such a mechanical stability will lead to a stable device performance. Fig. 9 shows the SEM images of the ITO and Ag NW/FZO composite TCEs after the bending test. Cracks are formed in the case of ITO as seen in Fig. 9(a), whereas no observable degradation in surface morphology is found in the case of Ag NW/FZO composite TCEs. The excellent flexibility of Ag NW/FZO composite electrode is mainly due to contribution of metallic Ag NWs with outstanding bending properties.[11] The role of FZO layer is forming effective fusions between Ag NWs at their numerous crossing points.

4. Conclusion

In conclusion, fully indium-free transparent and conductive Ag NW/FZO composite films with high haze were prepared at room

temperature on flexible substrates. By controlling the molecular weight of PVP and adding 18 μL EG solution of $AgNO_3$ (0.1 M) solution in advance, we can tune the Ag nanowire length from 15 μm to 60 μm. Using relative long (~60 μm) Ag NWs, we obtain pristine Ag NW mesh with sheet resistance of 19.2 Ω sq^{-1}, transmittance of 90.14% at 550 nm and haze of 38% by optimizing the spin coating ink concentration. Moreover, the post FZO layer deposition can effectively improve the conductivity of Ag NW mesh electrode by welding the NWs at the cross points. Furthermore, coating a FZO layer onto the Ag NW mesh is also expected to fill empty areas to contact to all over the active area of the device to allow for efficient charge extraction/injection, and strongly bind the Ag NW mesh to the flexible substrate with good mechanical stability. But, the Ag NW/FZO electrodes show decreasing transparency with the FZO layer increasing and the optimal thickness is about 100 nm in terms of FoM. Furthermore, we demonstrated that Ag NW/FZO films could be used as transparent electrodes for perovskite solar cells, which shows better results comparable to the reference devices on FTO substrates. These results lead to the conclusion that such composite electrode is a future-oriented electrode, exhibiting excellent flexibility, all room-temperature process, and higher tolerance to bending stress than the conventional ITO film as well as strong adhesiveness, which the pristine Ag NW mesh electrodes lacked.

Acknowledgements

This work is supported by NSFC (11174112, 51472110) and Shandong Provincial Science Foundation for Disguised Youth Scholars (JQ201214). The research programs from Ministry of Education, China, are also acknowledged (NCET-11-1027, 213021A). BC thanks the Taishan Scholar Professorship (TSHW20091007) tenured at University of Jinan.

References

1 K. H. Choi, J. Kim, Y. J. Noh, S. I. Na and H. K. Kim, *Sol. Energy Mater. Sol. Cells*, 2013, **110**, 147–153.
2 S. Jung, S. Lee, M. Song, D. G. Kim, D. S. You, J. K. Kim, C. S. Kim, T. M. Kim, K. H. Kim, J. J. Kim and J. W. Kang, *Adv. Energy Mater.*, 2014, **4**, 1–8.
3 J. Lee, P. Lee, H. Lee, D. Lee, S. S. Lee and S. H. Ko, *Nanoscale*, 2012, **4**, 6408–6414.
4 K. Ellmer, *Nat. Photonics*, 2012, **6**, 809–817.
5 T. Kim, A. Canlier, G. H. Kim, J. Choi, M. Park and S. M. Han, *ACS Appl. Mater. Interfaces*, 2013, **5**, 788–794.
6 M. Zhang, S. Fang, A. A. Zakhidov, S. B. Lee, A. E. Aliev, C. D. Williams, K. R. Atkinson and R. H. Baughman, *Science*, 2005, **309**, 1215–1219.
7 T. L. Chen, D. S. Ghosh, V. Mkhitaryan and V. Pruneri, *ACS Appl. Mater. Interfaces*, 2013, **5**, 11756–11761.
8 Y. H. Kahng, M. K. Kim, J. H. Lee, Y. J. Kim, N. Kim, D. W. Park and K. Lee, *Sol. Energy Mater. Sol. Cells*, 2014, **124**, 86–91.
9 P. Lee, J. Lee, H. Lee, J. Yeo, S. Hong, K. H. Nam, D. Lee, S. S. Lee and S. H. Ko, *Adv. Mater.*, 2012, **24**, 3326–3332.
10 L. B. Hu, H. S. Kim, J. Y. Lee, P. Peumans and Y. Cui, *ACS Nano*, 2010, **4**, 2955–2963.
11 H. J. Lee, J. H. Hwang, K. B. Choi, S. G. Jung, K. N. Kim, Y. S. Shim, C. H. Park, Y. W. Park and B. K. Ju, *ACS Appl. Mater. Interfaces*, 2013, **5**, 10397–10403.
12 T. G. Chen, B. Y. Huang, H. W. Liu, Y. Y. Huang, H. T. Pan, H. F. Meng and P. Yu, *ACS Appl. Mater. Interfaces*, 2012, **4**, 6857–6864.
13 J. Y. Lee, S. T. Connor, Y. Cui and P. Peumans, *Nano Lett.*, 2008, **8**, 690–692.
14 Y. G. Sun, Y. D. Yin, B. T. Mayers, T. Herricks and Y. N. Xia, *Chem. Mater.*, 2002, **14**, 4736–4745.
15 S. Zhu, Y. Gao, B. Hu, J. Li, J. Su, Z. Fan and J. Zhou, *Nanotechnology*, 2013, **24**, 335202.
16 K. Zilberberg, F. Gasse, R. Pagui, A. Polywka, A. Behrendt, S. Trost, R. Heiderhoff, P. Görrn and T. Riedl, *Adv. Funct. Mater.*, 2014, **24**, 1671–1678.
17 R. Zhu, C. H. Chung, K. C. Cha, W. B. Yang, Y. B. Zheng, H. P. Zhou, T. B. Song, C. C. Chen, P. S. Weiss, G. Li and A. Y. Yang, *ACS Nano*, 2011, **5**, 9877–9882.
18 Y. Liu, Q. Chang and L. Huang, *J. Mater. Chem. C*, 2013, **1**, 2970.
19 W. Gaynor, G. F. Burkhard, M. D. McGehee and P. Peumans, *Adv. Mater.*, 2011, **23**, 2905–2910.
20 E. Voroshazi, B. Verreet, T. Aernouts and P. Heremans, *Sol. Energy Mater. Sol. Cells*, 2011, **95**, 1303–1307.
21 C. H. Chung, T. B. Song, B. Bob, R. Zhu and Y. Yang, *Nano Res.*, 2012, **5**, 805–814.
22 A. Kim, Y. Won, K. Woo, S. Jeong and J. Moon, *Adv. Funct. Mater.*, 2014, **24**, 2462–2471.
23 J. Ajuria, I. Ugarte, W. Cambarau, I. Etxebarria, R. T. Zaera and R. Pacios, *Sol. Energy Mater. Sol. Cells*, 2012, **102**, 148–152.
24 T. Stubhan, J. Krantz, N. Li, F. Guo, I. Litzov, M. Steidl, M. Richter, G. J. Matt and C. J. Brabec, *Sol. Energy Mater. Sol. Cells*, 2012, **107**, 248–251.
25 Z. Q. Fang, H. L. Zhu, Y. B. Yuan, D. H. Ha, S. Z. Zhu, C. Preston, Q. X. Chen, Y. Y. Li, X. G. Han, S. G. Lee, G. Chen, T. Li, J. Munday, J. S. Huang and L. B. Hu, *Nano Lett.*, 2013, **14**, 765–773.
26 C. Preston, Y. Xu, X. Han, J. N. Munday and L. B. Hu, *Nano Res.*, 2013, **6**, 461–468.
27 C. Preston, Z. Fang, J. Murray, H. Zhu, J. Dai, J. N. Munday and L. B. Hu, *J. Mater. Chem. C*, 2014, **2**, 1248–1254.
28 D. Chen, X. Qiao, X. Qiu, J. Chen and R. Jiang, *J. Mater. Sci.: Mater. Electron.*, 2010, **22**, 6–13.
29 A. Yella, L.-P. Heiniger, P. Gao, M. K. Nazeeruddin and M. Grätzel, *Nano Lett.*, 2014, **14**, 2591–2596.
30 Y. G. Sun, B. Gates, B. Mayers and Y. N. Xia, *Nano Lett.*, 2002, **2**, 165–168.
31 R. M. Mutiso, M. C. Sherrott, A. R. Rathmell, B. J. Wiley and K. I. Winey, *ACS Nano*, 2013, **7**, 7654–7663.
32 J. Jiu, T. Araki, J. Wang, M. Nogi, T. Sugahara, S. Nagao, H. Koga, K. Suganuma, E. Nakazawa, M. Hara, H. Uchida and K. Shinozaki, *J. Mater. Chem. A*, 2014, **2**, 6326.
33 C. Seager and G. Pike, *Phys. Rev. B: Solid State*, 1974, **10**, 1435–1446.

34 S. M. Bergin, Y. H. Chen, A. R. Rathmell, P. Charbonneau, Z. Y. Li and B. J. Wiley, *Nanoscale*, 2012, **4**, 1996–2004.
35 A. Kim, Y. Won, K. Woo, C. H. Kim and A. J. Moon, *ACS Nano*, 2013, **7**, 1081–1091.
36 C. H. Liu and X. Yu, *Nanoscale Res. Lett.*, 2011, **6**, 75.
37 J. Han, P. Zhang, H. B. Gong, X. P. Yang, Z. W. Qiu, M. Zi and B. Q. Cao, *Acta Phys. Sin.*, 2013, **62**, 216102.
38 G. Haacke, *J. Appl. Phys.*, 1976, **47**, 4086–4089.
39 D. Wan, F. Huang, Y. Wang, X. Mou and F. Xu, *ACS Appl. Mater. Interfaces*, 2010, **2**, 2147–2152.
40 J. Burschka, N. Pellet, S. J. Moon, R. Humphry-Baker, P. Gao, M. K. Nazeeruddin and M. Gratzel, *Nature*, 2013, **499**, 316–319.
41 M. Liu, M. B. Johnston and H. J. Snaith, *Nature*, 2013, **501**, 395–398.
42 G. E. Eperon, V. M. Burlakov, P. Docampo, A. Goriely and H. J. Snaith, *Adv. Funct. Mater.*, 2014, **24**, 151–157.
43 J. M. Ball, M. M. Lee, A. Hey and H. J. Snaith, *Energy Environ. Sci.*, 2013, **6**, 1739.
44 J. H. Heo, S. H. Im, J. H. Noh, T. N. Mandal, C.-S. Lim, J. A. Chang, Y. H. Lee, H.-j. Kim, A. Sarkar, M. K. Nazeeruddin, M. Grätzel and S. I. Seok, *Nat. Photonics*, 2013, **7**, 486–491.
45 D. Liu and T. L. Kelly, *Nat. Photonics*, 2013, **8**, 133–138.

